JOURNAL OF THERMOPHYSICS AND HEAT TRANSFER
Vol. 21, No. 3, July–September 2007

Effect of Morphology of Carbon Nanotubes on Thermal Conductivity Enhancement of Nanofluids

Bong Hun Kim*
Daegu University, Geoyngsan, Geoyngbuk 712-714, Republic of Korea
and
G. P. Peterson†
University of Colorado at Boulder, Boulder, Colorado 80303

DOI: 10.2514/1.18341

An experimental study was conducted to investigate the effect of the morphology of carbon nanotubes on the thermal conductivity of suspensions. Three different types of carbon nanotubes, classified by aspect ratio as well as their aqueous suspensions, were prepared and characterized through the analyses of Raman spectroscopy: thermogravimetric analyzer, scanning electron microscopy, and transmission electron microscopy. The effective thermal conductivities of the samples were measured using a steady-state cut bar apparatus method. Enhancements based on the thermal conductivity of the base fluid are presented as functions of both the volume fraction and the temperature. Although functionalized single-walled nanotubes produced a more stable and homogeneous suspension, the addition of small amounts of surfactant to suspensions of "as produced" single-walled nanotubes demonstrated a greater increase in effective thermal conductivity than functionalized single-walled nanotubes alone. The effective thermal conductivity enhancement corresponding to 1.0% by volume approached ≈10%, which was observed to be lower than expected but more than twice the value, 3.5%, obtained for similar tests conducted using aluminum oxide suspensions. However, for suspensions of multiwalled nanotubes, the degree of enhancement was measured to be approximately 37%. Comparison of the measured data and that predicted by a previously developed theoretical model indicated good agreement for a corresponding shape factor, *n*, of 12 for the single-walled nanotubes, whereas multiwalled nanotube suspensions were well matched when the shape factor was 36, indicating that extension of the theoretical model may allow it to be applied to carbon nanotube suspensions if the effect of clustering can be accurately predicted.

Nomenclature

A	=	area, cm^2
k	=	thermal conductivity, $W/cm \cdot K$
L	=	distance, cm
n	=	shape factor
q	=	heat transfer rate, W
T	=	temperature, °C
α	=	thermal conductivity ratio
γ	=	thermal expansion coefficient, $1/K$
ρ	=	density, g/cm^3
ϕ	=	volume fraction, %
ψ	=	sphericity
ω	=	empirical exponent

Subscripts

c	=	copper or cooler side
e	=	effective
f	=	base fluid
g	=	gap
h	=	heater
m	=	mean
o	=	O-ring

Received 22 June 2005; revision received 7 October 2005; accepted for publication 22 October 2005.

*Associate Professor, Automotive, Industrial and Mechanical Engineering Department.

†Professor and Chancellor, Mechanical Engineering Department. Fellow AIAA.

I. Introduction

SINCE the initial classical work of Maxwell [1] in 1904, numerous investigations of the high effective thermal conductivity of solid particle suspensions have been conducted [2–4]. Recent progress in nanotechnology has made possible the production of carbon nanotubes (CNTs) with unusually high thermal conductivities [5], and large-scale production methods for both single-walled nanotubes (SWNT) and multiwalled nanotubes (MWNT) have been developed and commercialized [6–8].

Choi et al. [9] measured the effective thermal conductivity of nanotubes in oil suspensions, using a transient hot-wire method at room temperature. MWNT produced by chemical vapor deposition (CVD) methods [8] were dispersed into alpha olefin oil with a volumetric loading of up to 1% by volume. The results indicated that the thermal conductivity ratio, defined as k_e/k_f, was nonlinear with the volume fraction and reached values of more than 2.5 at 1% by volume.

Xie et al. [10] presented effective thermal conductivities of MWNT suspensions in distilled water and ethylene glycol. A chemical treatment using various mixtures of nitric and sulfuric etchants was employed to ensure well-dispersed aqueous suspensions by forming hydrophilic functional groups on the surfaces of the "as produced" MWNT. The results indicated that the thermal conductivity enhancement, $(k_e - k_f)/k_f$, increased linearly with the volume fraction and indicated 7 and 13% improvement for suspensions in distilled water and ethylene glycol, respectively, at 1.0% volume fractions. Suspensions of functionalized MWNT demonstrated that the degree of enhancement decreased with increases in the thermal conductivity of the base liquid, which is similar to the trends observed for Al_2O_3 nanoparticle suspensions [11–13]. For the particular case of distilled water, the magnitude of the enhancement was significantly smaller than expected, when considering that the thermal conductivity of CNTs is higher than that of the fluids by three to four orders of magnitude [5].

Assael et al. [14] measured the effective thermal conductivity of "as produced" MWNT (CVD grown) suspensions in distilled water

using a transient hot-wire technique at room temperature. A surfactant, sodium dodecyl sulfate, was used to produce stable and uniform suspensions instead of the chemical treatment employed by Xie et al. [10]. This investigation studied the effect of both the surfactant concentration and the homogenization time (ultrasonication time) on the effective thermal conductivity. The results indicated that the homogenization time had a significant impact on the aspect ratio (defined as the ratio of length to diameter) with higher aspect ratios observed for shorter homogenization times and that the thermal conductivity enhancement increased with the aspect ratio. As a result, the highest enhancement was observed to be 38% (with an average value of 29%) for the samples with the shortest homogenization times demonstrating the greatest improvement. Wen and Ding [15] also recently presented an experimental study to investigate effective thermal conductivity of aqueous MWNT suspensions with volume concentration up to 0.84%. Results showed that the degree of enhancement ranged from 27 to 30% corresponding to the fluid temperatures, 25 and 45°C, respectively.

To date, the only theoretical models capable of predicting the effective thermal conductivity enhancement of CNT suspensions are those based on Fourier's law of heat conduction. Maxwell [1] first proposed an explicit equation for the effective thermal conductivity in terms of the thermal conductivity ratio, $\alpha = k_p/k_f$, and the volume fraction.

$$\frac{k_e}{k_f} = 1 + \frac{3(\alpha - 1)\phi}{(\alpha + 2) + (1 - \alpha)\phi} \tag{1}$$

This model does not include any variables that compensate for variations in the shape of the particles. Thus, the theoretical predictions show only minor conductivity increases, as indicated in Choi et al. [9] and the other previous studies employing Al_2O_3 or CuO nanoparticles [11–13]. Like Maxwell [1], Jaffrey [16] and Davis [17] developed theoretical models including higher order terms based on Fourier's law of heat conduction. These three models resulted in nearly identical predictions of the effective thermal conductivity, especially at low-volume fractions.

For CNT suspensions, an organized structure at the solid/liquid interface is another contributing factor in the effective thermal conductivity enhancement. Hamilton and Crosser [18] developed a theoretical model (HC model) in terms of the thermal conductivity ratio, $\alpha = k_p/k_f$, and the volume fraction and they added a new term, the shape factor

$$\frac{k_e}{k_f} = \frac{\alpha + (n-1) - (n-1)(1-\alpha)\phi}{\alpha + (n-1) + (1-a)\phi} : n = \frac{3}{\psi^{\omega}} \tag{2}$$

where ψ is 1 for spheres and 0.5 for cylinders and ω ranges from 1 to 2. However, these values were introduced and are applicable for chiplike particles with a low aspect ratio. In the present study, larger values (2 to 4) were introduced by considering configuration of CNTs with a much higher aspect ratio. When $\psi = 1$, the HC model is identical to Maxwell's. Prediction by the HC model ($n = 6$) significantly underestimated the measured data, as presented in Choi et al. [9] in which CNT suspensions in liquids having relatively low thermal conductivity, such as engine oil, were evaluated. Comparisons for CNT suspensions in distilled water, however, were not available.

In Lee et al. [12] the HC model, which did not include the effect of particle size, resulted in measured values that were much higher than those predicted, with the variation increasing with decreases in the size of the nanoparticles. Choi et al. [9] and Xie et al. [10] also found the measured data for CNT suspensions to be significantly greater than those predicted by the HC model. Wang et al. [11] presented similar results and suggested that any new models should include the effects of both the microscopic motion and particle size, because the previous models could not accurately predict the heat flow for particle suspensions at the nanometer scale.

Das et al. [19] suggested that the main mechanism of thermal conductivity enhancement could be the stochastic motion of the nanoparticles, such as the temperature dependent Brownian motion. At low temperatures, the enhancement due to this random motion would be negligible but would become more significant as the temperature increased.

As discussed previously, all of the existing theoretical models were derived from Fourier's law of heat conduction in both the liquid and the solid particles. Thus, the theoretical predictions are expected to show only a minor enhancement because heat flow in the CNT suspensions is governed only by the thermal conduction mechanism [9]. Choi et al. [9] suggested that the actual enhancement was a consequence of two separate phenomena: the ballistic heat conduction in the CNT and an organized structure at the interface. Because heat flow in CNT suspensions is limited by the interfacial thermal resistance, the assumption that this aligned solidlike structure could result in an enhanced heat flow is regarded as an answer to the question of why CNT suspensions demonstrated a significantly enhanced thermal conductivity. This mechanism may, in fact, play an important role in the thermal conductivity enhancement, because the liquids adjacent to the CNT with extremely small diameters, especially SWNT, tend to constitute a solidlike layered structure.

This idea, however, is somewhat contradictory to the main mechanism, microconvection due to Brownian motion, as presented in Wang et al. [11] and Lee et al. [12]. Xie et al. [10] noted that the idea of layered structures had not been verified and thus, was still open to debate. The contribution due to the ballistic heat conduction has been treated as a somewhat less important factor, due to the organized structure at the interface and the fact that it lacks theoretical considerations based on the morphology of CNT [9].

Motivation for the current investigation results from the need to investigate the effect of morphology, especially the shape factor, i.e., the aspect ratio and carbonaceous structure of CNTs on the thermal conductivity enhancement. Although a number of studies have investigated the thermal conductivity of CNT suspensions and compared the measured data with those predicted by the HC model, none of these have presented experimental data for different kinds of CNTs. In the current investigation, CNT suspensions, divided into a matrix of three sample suspensions and three different values of aspect ratios, are used to show the quantitative relationship between the thermal conductivity enhancement and the aspect ratio. In addition, the thermal conductivities were measured at an elevated temperature to examine the effect of temperature. A parametric study was conducted to investigate the effect of morphology of CNTs on the effective thermal conductivity of suspensions as functions of both the volume fraction and the temperature. To accomplish these objectives, the thermal conductivities of the individual suspensions were measured using a steady-state method, similar to the methods employed by Challoner and Powell [20].

II. Preparation and Characterization of Carbon Nanotube Suspensions

The CNTs employed in the present work were classified as CNT A, "as produced" SWNT (CVD grown) [6] provided by Carbon Nanotechnologies, Inc.; CNT B, functionalized SWNT (arc generated) [21,22] provided by Carbon Solution, Inc.; and CNT C, purified MWNT (CVD grown) provided by MER Corp.

The internal graphite structures of these CNT samples were qualitatively analyzed using Raman spectroscopy [23,24] with an argon laser. For all the CNT samples, Raman peaks (G peaks or tangential band) corresponding to crystalline graphite centered at 1580 cm^{-1}, but D peaks (disorder band) due to amorphous carbon, fine graphitic particles, or defects appeared near 1350 cm^{-1}. When compared with Raman spectra presented in Tohji et al. [25] the spectrum of CNT A, illustrated in Fig. 1a, was well matched with that of raw soot. However, CNT B in Fig. 1b demonstrated a much stronger peak at the disorder band (1350^{-1}) than the purified undamaged SWNT of Tohji et al. [25]. This implies that the graphitic structure of CNT B had been changed by a chemical treatment designed to obtain a hydrophilic functional group on the surface, or as a by-product of the chemical treatment, amorphous carbons were formed on the outer surface of the SWNT [26].

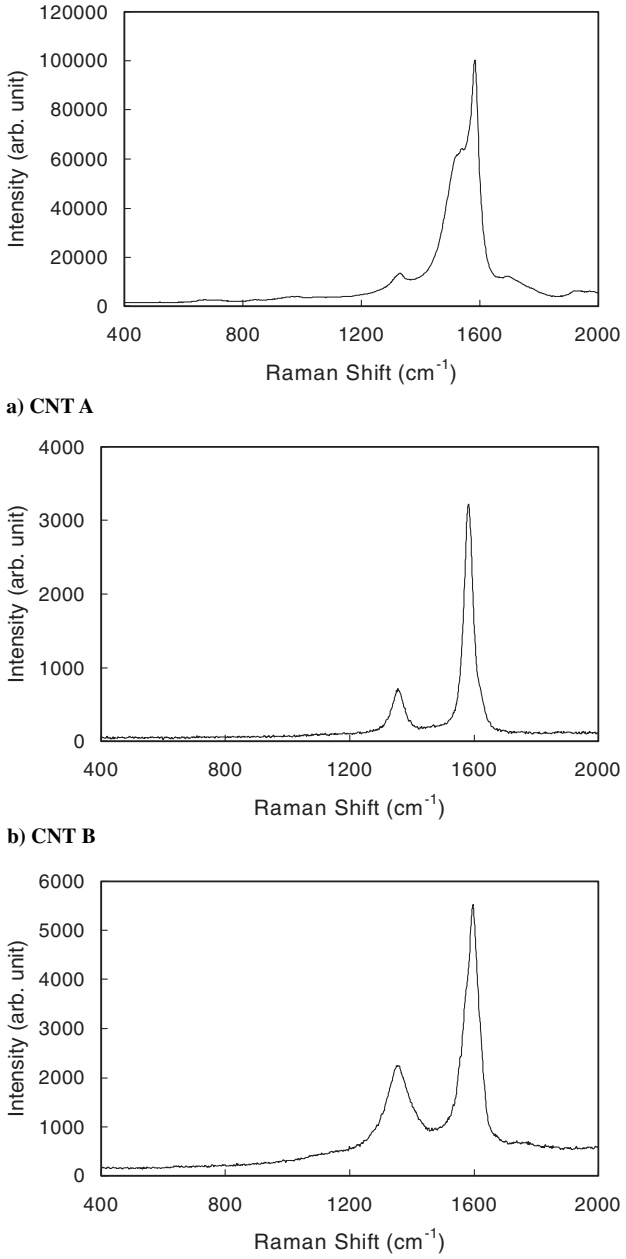

Fig. 1 Raman spectra of CNT powders.

Similar to Rinzler et al. [27] and Chiang et al. [28] the purity of the three CNT were characterized through analysis of the reactivities obtained by the thermogravimetric analyzer (TGA). In all the tests, dry air was used to oxidize the CNT samples. The rate of temperature rise was maintained at 5°C/ min to a level of 950°C after having been held for 1.5 h at 150°C to remove moisture from the sample. The TGA data show a correlation between the temperature of the air oxidation (the burning temperature) and carbonaceous structure of the sample [29].

Figure 2 indicates that the burning temperature of CNT A was approximately 550°C, which was almost identical to the corresponding value (≈550°C) of CNT B. The results showed a good agreement with Rinzler et al. [27]. However, the "as produced" SWNT demonstrated a broader burning temperature range, due to the presence of some unwanted carbonaceous materials and nanoparticles with catalyst metals (Ni or Co, etc.). As expected, the highest burning temperature was approximately 700°C for CNT C, purified MWNT [27].

Suspensions of the three CNTs were characterized using scanning electron microscopy (SEM) by visualizing the CNTs dispersed in distilled water, as shown in Fig. 3. To characterize the samples in this

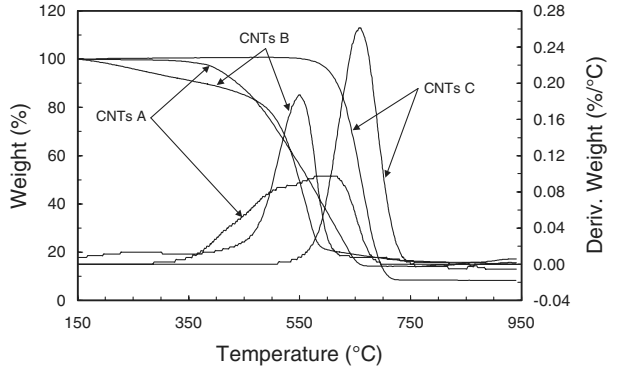

Fig. 2 TGA of CNT powders.

way, it was necessary to produce stable and well-dispersed samples. A small amount of both CNTs (in the case of samples A and C) and a surfactant (sodium dodecyl benzene sulfonate: SDBS) was mixed with distilled water and then ultrasonicated for 10 min (2 repetitions of 5-min sonication) [30]. No surfactant was used for CNT B, the functionalized SWNT. A drop of liquid sample was put on a piece of silicon wafer and uniformly coated using a spinning coater and dryer.

The SEM photographs shown in Fig. 3b verified that the functionalized SWNT of CNT B was well dispersed and very uniform in both diameter and length. The average length was estimated to be ≈1.5 μm. In the same way, nanotube bundles for CNT A and C, shown in Fig. 3a and 3c, respectively, were properly disentangled by the surfactant and found to be uniformly dispersed. The average length of CNT A and C was approximately 3 and 30 μm, respectively.

The range of diameters was measured using a transmission electron microscopy (TEM) at 100 kV. To prepare the TEM samples, the SEM samples were diluted in ethanol and placed onto a lacey carbon TEM grid [28]. The TEM photographs shown in Figs. 4a and 4b indicate that the mean diameters of CNT A and CNT B were approximately 20 and 15 nm, respectively, in a range of 10 to 35 nm. The MWNT of CNT C shown in Fig. 4c were thicker than the SWNT and had a mean diameter of approximately 90 nm, which corresponded well with the information presented by Assael et al. [14].

Nine different samples of CNT suspensions were prepared and evaluated to determine the effective thermal conductivity. The three different nanotubes, CNT A, B, and C, were dispersed into distilled water and ultrasonicated for 20 min (4 repetitions of 5-min sonication) using a probe-type sonicator (VCX750, Sonics & Materials, Inc.) with three different loadings, 0.3, 0.7, and 1.0% by volume. As was the case for the SEM and TEM samples, a surfactant (SDBS) was added to the suspensions of CNT A and C to produce stable and homogeneous samples. The surfactant ratio to CNTs was 1:1 by mass. For these samples, the volume fraction is defined as

$$\phi = \left(\frac{m_p/\rho_p}{m_p/\rho_p + m_f/\rho_f} \right) \tag{3}$$

Here, ρ_p corresponds to the density of SWNT and MWNT, and the values of 1.3 and 2.2 g/cm^3, respectively, were assigned in the current study. As is normally the case, the density of the SWNT varies with the crystalline structure, ranging from 1.3 to 1.4 and from 2.2 to 2.6 for the MWNT [31,32].

III. Experimental Apparatus

Figure 5 illustrates a schematic of the test facility, which is composed of two copper rods aligned axially in the vertical direction. An O-ring is located between the rods, to form a cell to contain the CNT nanofluids. As illustrated, both the upper and lower rods are 115 mm long and have an external diameter of 26 mm. A small duct, 0.6 mm in diameter, was machined on each side to allow the test fluid to be inserted into the cell. At the top end of the upper rod, a band-type electric heater (110 Ω) was installed and connected to a dc

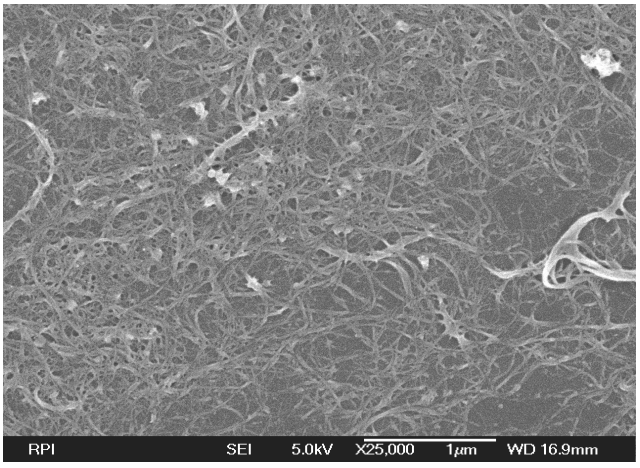

a) CNT A

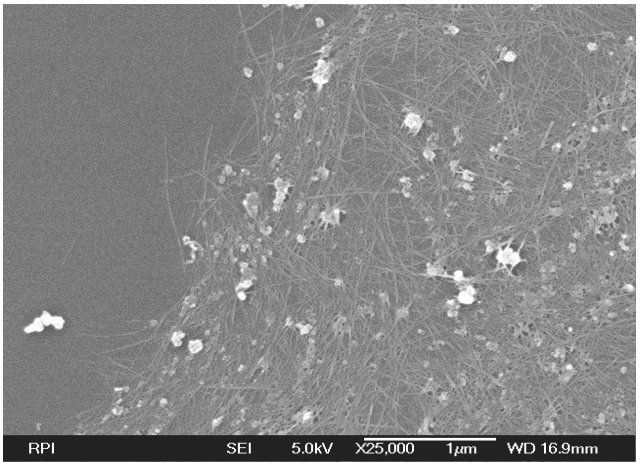

b) CNT B

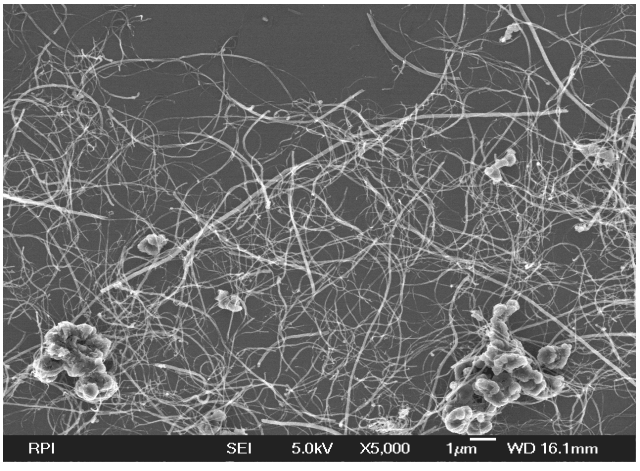

c) CNT C

Fig. 3 SEM photographs of CNT suspensions.

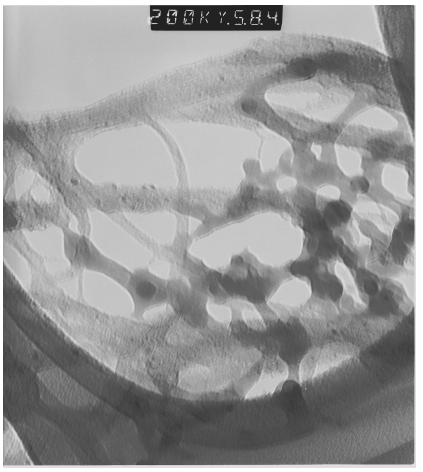

a) CNT A

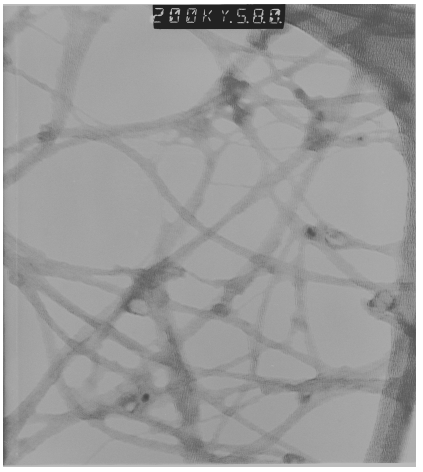

b) CNT B

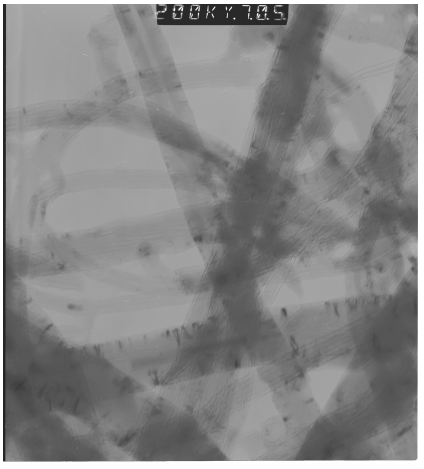

c) CNT C

Fig. 4 TEM photographs of CNT suspensions.

power supply, and the bottom end of the lower rod was cooled using fluid from a constant temperature bath.

Fourteen K-type thermocouples (0.5 mm in diameter) were used to monitor and measure the temperature. The thermocouples, paired in T9/T10 and T11/T12, were placed in the holes drilled to the centerline of the rods to measure the axial temperature difference. In the same way, four pairs of thermocouples (T1/T5, T2/T6, T3/T7, and T4/T8) were installed at positions adjacent to the upper and lower surfaces of the cell.

During the experiment, the two rods were compressed axially to maintain a cell height of 1.7 mm, and the entire facility was then placed in a vacuum chamber and held at a vacuum of less than 0.02 torr. The thermocouples were all connected to a data logger, interfaced with a personal computer, and the measured data were recorded at 8 s intervals.

Using an internal reference junction, the temperature was measured with an uncertainty of less than 0.5% over a temperature range of −10 to 100°C; however, the error involved in the temperature difference (using a fixed reference junction) was found

to be less than 0.02°C. Because of the importance of the accuracy of these measurements on the calculation of axial heat flux, care was taken to ensure the accuracy of the instruments. The combination of the instrumentation and sensors used, resulted in an overall uncertainty of 1.0% in the temperature measurements and 1.5% in the thermal conductivity measurements.

IV. Test Conditions and Procedures

The cell bounded by the two ends of the copper rods and by the O-ring, as shown in Fig. 5, was charged with approximately 0.5 cm^3 of the test nanofluids, and then both the inlet and outlet tubes were sealed. The test facility was placed in the vacuum chamber and subjected to an initialization process that required approximately 12 h to reach steady-state, defined as the point where the temperature variation was less than 0.1°C and the pressure in the vacuum chamber was less than 0.02 torr.

After the initialization process, the coolant, which was maintained at −15°C, was allowed to flow through the cooling jacket shown in Fig. 5, and the flow rate was regulated at 1.3 gal/min. At the same time, the heater was activated and the power incremented in a stepwise fashion. At each step, the system was allowed to reach a steady state, and then the process was repeated, providing a data set that allowed the effective thermal conductivity to be determined as a function of temperature for a given volume fraction. This process was then repeated until three complete sets of data had been obtained for a given volume fraction of the various nanofluids. The process took approximately three days for each sample and helped to verify the stability of the sample suspensions. To enhance the accuracy of the measurements, the final data were reduced from 15-min temporal averaging at each steady-state condition.

The axial heat transfer rate was determined using the average axial temperature difference in the heated and cooled sides as

$$\Delta T_c = (T_{10} - T_9 + T_{11} - T_{12})/2 \tag{4}$$

$$q = A_c k_c \frac{\Delta T_c}{L_c} \tag{5}$$

Using the thermal conductivity of copper, which was estimated from the temperature-dependent approximation [32]

$$k_c = 4.06 - 0.08\frac{(T-2)}{75} \tag{6}$$

The effective thermal conductivity could be determined from a one-dimensional heat conduction equation, which included the thermal resistance of the O-ring as

$$k_e = \frac{1}{A_f}\left(\frac{qL_g}{\Delta T_g} - k_o A_o\right) \tag{7}$$

where ΔT_g represented the temperature difference experienced by the test fluids and was estimated by averaging the four values of the temperature differences:

$$\Delta T_g = (T_1 - T_5 + T_2 - T_3 + T_3 - T_7 + T_4 - T_8)/4 \tag{8}$$

The thermal conductivity of the O-ring was estimated to be 5.0×10^{-4} W/cm · K [32], based upon preliminary experiments performed with no fluid present in the cell. The cell height, L_g, in Eq. (6) should be adjusted for thermal expansion using the mean temperature of the copper rods in both the heated and cooled sides

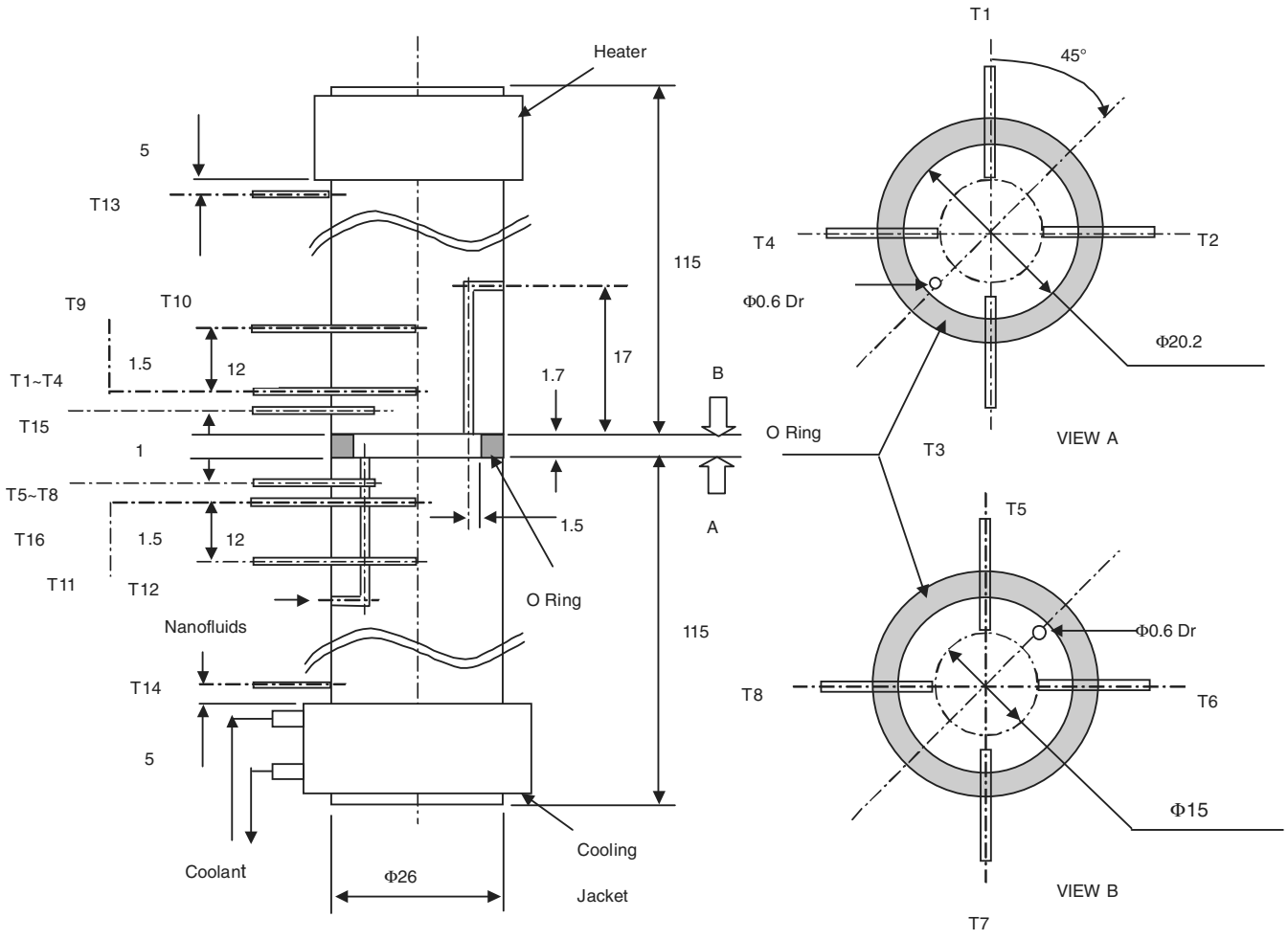

Fig. 5 Experimental apparatus.

$$L_g = \gamma L(\bar{T}_h - \bar{T}_c) \tag{9}$$

where γ is 1.6×10^{-5} (K^{-1}) for the current investigation [33]. The mean temperatures of the copper rods were determined as

$$\bar{T}_h = (T_9 + T_{13})/2 \tag{10}$$

and

$$\bar{T}_c = (T_{11} + T_{14})/2 \tag{11}$$

The enhancement of the effective thermal conductivity was defined as a percent, $(k_e - k_f) \times 100/k_f$, as a function of the mean fluid temperature:

$$T_m = (T_{15} + T_{16})/2 \tag{12}$$

V. Results and Discussion

The effective thermal conductivity of nine different CNT nanofluids was measured, using a one-dimensional steady-state method. As described in Eq. (7), the thermal conductivity was calculated using the measured axial heat transfer, Eq. (5), and the temperature difference across the fluid cell, Eq. (8). Before the initiation of the formal experimental program, several preliminary tests were conducted to calibrate and verify the validity of the test facility. As illustrated in Fig. 6, the effective thermal conductivity of distilled water was measured as a function of temperature. The linear fit of the measured data demonstrated an increasing trend with temperature and was in good agreement with the property data as reported in the literature [34] with an average deviation of less than 1%. From the measured data, a linear equation for k_f as a function of T_m was developed and is presented here as Eq. (12).

Figure 7 illustrates the enhancement of the effective thermal conductivity for the case of CNT B, functionalized SWNT, for volume fractions of 0.3, 0.7, and 1.0%. The resulting variation in the enhancement, defined as $(k_e - k_f)/k_f$, was analyzed as a function of the temperature and adjusted for the input power as determined from the voltage supplied to the power supply. The overall trend indicated that the magnitude of enhancement tended to increase with temperature for a given volume fraction, except for the case of 0.3.%. All of the curves were shifted toward a lower temperature as the degree of enhancement increased, demonstrating a consistency with principles of thermal conductivity. For the lowest volume fraction, 0.3%, the enhancement was found to be nearly insensitive to temperature.

The well-dispersed suspensions of SWNT result in a liquid cell with a layered structure making the heat flow at the interface effective [9]. Careful examination of the reductions in the thermal conductivity [5] of CNTs with temperature indicates that there may exist an additional contribution to the enhancement across the solid/liquid interface at elevated temperatures. Although the microconvection due to Brownian motion enhances the heat flow at elevated temperatures [19], the contribution may be too small to overshadow the degradation of the thermal conductivity caused by the relatively smaller CNT bundles usually observed in functionalized CNTs with low volume fractions. The effect of the temperature became easily recognizable, however, once the volume fraction was increased. This is consistent with the experimental results of Das et al. [19], who reported significant increases in the enhancement of the thermal conductivity with temperature for nanofluids containing aluminum oxide with volume fractions up to 4%.

Higher volume fractions of SWNT tended to form larger sized clusters or aggregates and demonstrated characteristics that closely resembled the behavior of micron-sized suspensions. Although the contribution of the microconvection increased with increased temperature, because the agglomerate size approximated micron-sized suspensions, the contribution of the ballistic heat conduction did not appear to be an important factor when considering the variation in the thermal conductivity of the nanotubes [9].

For a volume fraction of 1.0%, Das et al. [19] found that the enhancement increased by approximately 8% as the temperature changed from 25 to 50°C but increased less than 2% in the case of CNT B, as shown in Fig. 7. Although the effect of temperature was not significant, the maximum enhancement corresponding to a volume fraction of 1.0% of CNT B approached 10%, which was observed to be more than twice the value, 3.5%, obtained in the case of aluminum oxide nanofluids [10,11]. When considering the very high thermal conductivity of CNTs, 20 $W/cm \cdot K$, the enhancement of CNT B, functionalized SWNT, was somewhat lower than expected.

In Fig. 8, the thermal conductivity enhancement of CNT A, as produced SWNT, was presented as a function of the temperature and volume fraction. Variations of the enhancement demonstrated a similar trend to that observed in CNT B; however, the data were shifted upward by 1 to 2%. Thus the maximum enhancement corresponding to a volume fraction of 1.0% reached approximately 11%. It is interesting to note that CNT A demonstrated an equivalent

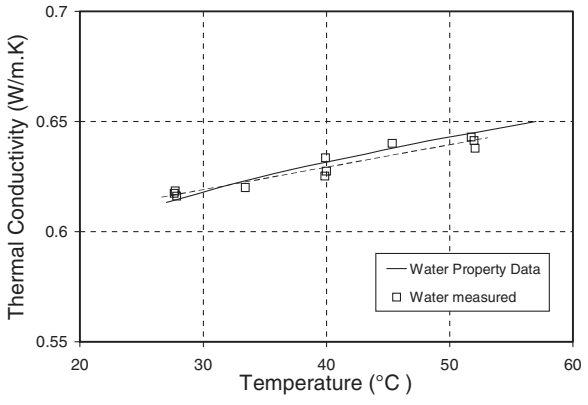

Fig. 6 Validation of present steady-state method to measure thermal conductivity of distilled water.

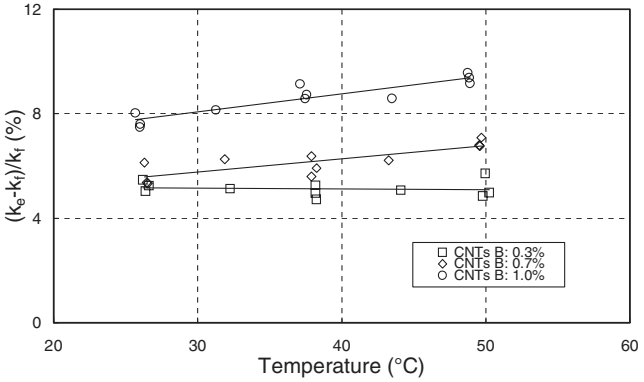

Fig. 7 Variation of the thermal conductivity enhancement of CNT B.

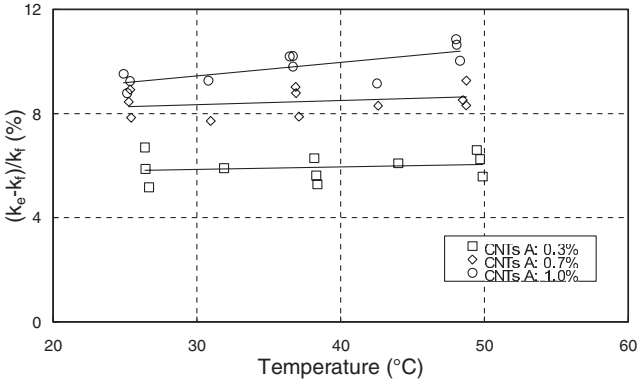

Fig. 8 Variation of the thermal conductivity enhancement of CNT A.

or slightly higher degree of enhancement, given that it contained significantly more impurities [6,7] than CNT B, as shown in the TGA analysis. This implies that suspensions of CNT A with a surfactant SDBS proved to be more advantageous than CNT B in terms of the effective thermal conductivity, in spite of the fact that the CNT B resulted in more stable and homogeneous suspensions than CNT A.

Examination of the Raman scattering and SEM/TEM photography can help to explain this apparent anomaly. Strong D peaks in the Raman scattering shown in Fig. 1b indicate that the surface of CNT B is transformed into hydrophilic carbonaceous graphite containing inherent defects [26–28], which may result in a larger thermal resistance in both the axial and radial directions. In addition, the SEM/TEM photography of CNT B samples indicated a mean diameter of 15 nm and a length of 1.5 μm, which was both thinner and shorter than CNT A that typically had a diameter of 20 nm and a length of 3 μm. The smaller CNTs led to larger surface areas that were more likely to form an aligned solidlike structure at the interface [9]. Although the organized structure increased the effectiveness of the heat flow, changes in the surface morphology overshadowed the contribution of the organized structure to the heat flow across the interface. In addition, the CNTs with a lower aspect ratio may result in smaller sized CNT bundles, which are more dominant in the case of functionalized CNTs. The combination of reduction of the diameter and the small bundle size may cause degradation in the heat flow in both the axial direction of the individual CNT and in the lateral direction of the individual bundles. In this sense, the functionalized CNTs may be less advantageous than the as produced case, even when another mechanism, ballistic heat conduction, is taken into consideration.

The thermal conductivity enhancement of CNT C suspensions are presented in Fig. 9 as a function of temperature for the given volume fractions. Overall the trend indicated that the degree of enhancement increases linearly with temperature and nonlinearly with volume fraction. This trend is similar to that observed by Choi et al. [9] in which the measured effective thermal conductivity of MWNT suspensions in alpha olefin oil demonstrated a similar nonlinear trend with respect to the volume fraction. As was the case for the SWNT suspensions, all of the data shifted toward a lower temperature as the degree of enhancement increased. At the same heat input, the mean temperature of the fluid was reduced approximately 3°C for the variation of the volume fraction ranging from 0.3 to 1.0%. It was demonstrated that the effect of temperature was more significant than for the SWNT suspensions. As shown in Fig. 9, the increases in enhancement were in the range of 5 to 6%, which was nearly double that observed in CNT A and B, for the range of temperatures evaluated. The contribution of convection, due to the Brownian motion, may be larger than that required to compensate for the degradation of the thermal conductivity, as both temperature and volume fraction increased.

All the data, however, exhibited the same rate of increase with temperature, especially at the low volume fraction, 0.3%, where the rate of enhancement increase with respect to temperature was nearly the same as that observed at a volume fraction of 1.0%. This observation is very different from that observed for CNT A and B, the SWNT suspensions. This implies that there may be a more dominant mechanism than microconvection that is dependent upon the volume fraction. If the microconvection is the principal mechanism governing the heat flow, the rate of increase in enhancement with temperature should increase as the volume fraction increases, as was shown in the SWNT samples.

It is interesting at this point to relate the thermal enhancement to the diameter of the CNTs, which was 5 times larger than those used in CNT A and B. In suspensions containing large diameter CNTs, the contribution of the layered structure at the interface may be less dominant than expected from the other mechanisms of heat transfer, i.e., ballistic conduction and clustering or aggregation. As mentioned above, the effect of clustering [10,35] may be significant in the case of CNT C with large diameters and high aspect ratios because the CNT bundles are so large that they are already interconnected even at low volume fractions such as 0.3%.

The maximum enhancement corresponding to a volume fraction of 1.0% and the highest heat input was found to be approximately 37%. Compared with the thermal conductivity enhancement measured in Xie et al. [10], the present data showed an increase almost 5 times larger at the same temperature, 25°C. The discrepancy in the measured results may result from the fact that the CNT used in Xie et al. [10] was 15 nm in diameter and 30 μm long and was chemically treated to form a hydrophilic functional group on the surface. Although the aspect ratio was larger than that used in the present study, the degree of enhancement was quite low, due to both a smaller diameter and the chemically treated surface.

In addition, the measured data of Assael et al. [14] and Wen and Ding [15] were compared with the present data. Assael et al. [14] attempted to determine the effect of homogenization time (or time of ultrasonication) on the effective thermal conductivity and reported an approximate 29% enhancement, which was an average of the measured data ranging from 20 to 38% for a volume fraction of 0.6 %, whereas Wen and Ding [15] showed nearly the same degree of enhancement ($\approx$30%) in spite of the larger volume fraction (0.84%) and higher fluid temperature (45°C). However, data corresponding to both studies were located between the curves corresponding to the CNT C with volume fractions between 0.7 and 1.0%. Assael et al. [14] indicated that maximum enhancement was obtained for the minimum time of ultrasonication, 20 min. As the homogenization time increased, the enhancement also decreased, indicating that the effect of clustering and aspect ratio on the thermal conductivity enhancement may have been partially overlooked in Assael et al. [14].

In Fig. 10, the thermal conductivity enhancement for the given temperature, 25°C, was presented as a function of the volume fraction and was compared with that predicted by the HC model with different shape factors. Here, the sphericity in Eq. (2) was 0.5 (for cylinders) [17] and ω was chosen to range from 2 to 4, which caused the shape factor to vary from 12 to 48. This empirical exponent could represent the effect of clustering on heat flow in CNT suspensions. By assigning larger values than those [17] employed in micron-sized mixtures, it may be possible to describe the mechanisms that govern

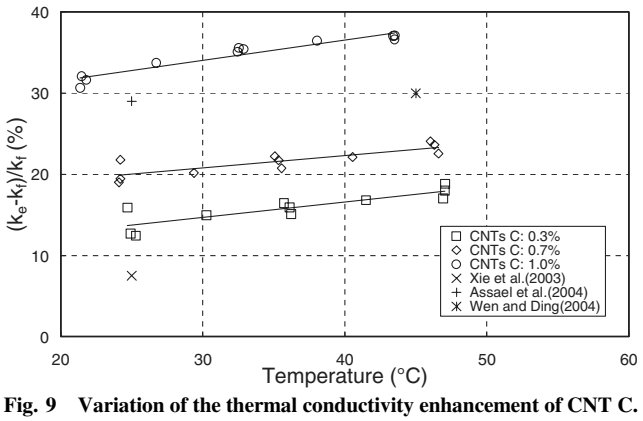

Fig. 9 Variation of the thermal conductivity enhancement of CNT C.

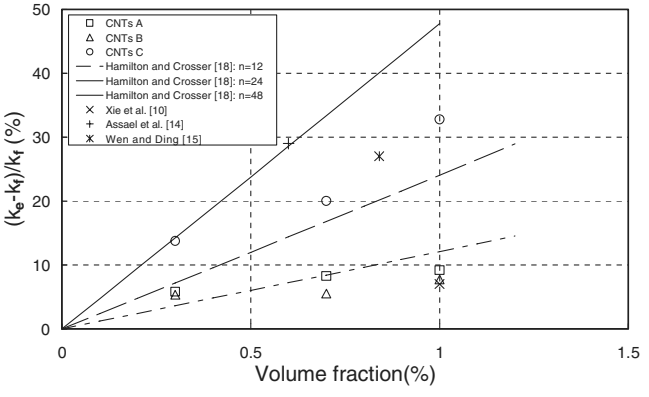

Fig. 10 Comparison of the measured data and prediction by the HC model.

the thermal conductivity enhancement for the CNT suspensions containing large sized clusters or aggregates.

To examine the effect of aspect ratio on the enhancement, measured data were classified into three different groups according to the magnitudes of the aspect ratio. The characterization of CNT suspensions using SEM/TEM photography indicated that the sample suspensions CNT A, B, and C had aspect ratios of 150, 100, and 330, respectively. As shown in Fig. 10, CNT B, functionalized SWNT, showed the lowest degree of enhancement, whereas the highest degree was observed in CNT C, MWNT suspensions. When considering the morphology of these CNTs it was clear that the overall trend indicated a good agreement with the effects of the aspect ratio, which was presumed to be closely related to the bundle size, indicating that the degree of enhancement increased with aspect ratio. However, Xie et al. [10] showed much lower enhancement than expected, despite the high aspect ratios studied ($\approx$2000), in all likelihood, due to the degradation of the CNTs discussed previously. A least-squares fit line through the measured data of SWNT suspensions CNT A and B was observed to closely match the curve predicted by the HC model with $n = 12$. An alternative curve corresponding to $n = 36$, in the middle of the two curves resulting from the HC model with $n = 24$ and $n = 48$, was shown to predict the measured data for CNT C and the data of Assael et al. [14] and Wen and Ding [15] reasonably well. As discussed before, the shape factor is closely related to the aspect ratio and can serve as an indication of the effect of cluster size on the extended HC model, making it applicable to CNT suspensions. As the CNT bundles become larger in size and interconnect with neighboring bundles aligned in the heat flow direction, the aspect ratio increases. Such a bundle lattice in the preferred direction may constitute multiple passages for heat flow, which results in significant enhancement in the effective thermal conductivity.

VI. Conclusions

The effect of the morphology of CNT on the effective thermal conductivity of suspensions was investigated as a function of both the volume fraction and temperature. Test samples of SWNT with small amounts of surfactant SDBS provided a higher effective thermal conductivity than functionalized SWNT. The maximum enhancement for the SWNT corresponding to a volume fraction of 1.0% approached $\approx$10%, which was observed to be more than twice that of the other values, 3.5%, obtained in the case of aluminum oxide nanofluids.

The thermal conductivity enhancement of MWNT suspensions was shown to increase linearly with temperature but demonstrated a nonlinear increase with respect to the volume fraction. In addition, effects of temperature variations indicated that the enhancement may be attributed to the effect of clustering, which was found to be closely related to the bundle size and volume fraction. The maximum enhancement corresponding to a volume fraction of 1.0% was found to be approximately 37%, which was comparable to the values obtained in previous investigations. Further comparison of the experimentally measured data and that predicted by the HC model indicated that the SWNT suspensions were in good agreement with the values predicted by the extended HC model with $n = 12$. In previous studies, a value of $n = 36$ was necessary to achieve good correlation. As a result, the extended HC model may be applicable to CNT suspensions with certain qualifications. For example, as shown in Fig. 10, the enhancement is linearly depdendent on the volume fraction as the extended HC model predicts. However, the measured data demonstrate a nonlinear dependence, which the extended HC model fails to capture. Furthermore, the shape factor alone cannot account for other factors such as surface treatment, interfacial thermal resistance, or Brownian motion of nanoparticles as discussed in Sec. V.

The shape factor was shown to be closely related to the aspect ratio. As the aspect ratio increases, the CNT bundles become larger in size and interconnect with neighboring bundles aligned in the direction of the heat flow. These bundles form a lattice structure that constitutes multiple passages in the heat flow direction, resulting in significant enhancement in the thermal conductivity. Overall the results of this investigation indicate that the extended HC model may be applicable to CNT suspensions if the effect of clustering can be accurately predicted.

Acknowledgments

This work was partly supported by the Faculty Research Program of Daegu University and the National Science Foundation. The advice and encouragement of Robert Vajtar and P. M. Ajayan, both from Rensselaer Polytechnic Institute, is very much appreciated.

References

[1] Maxwell, J. C., *Electricity and Magnetism, Part 2*, 3rd ed., Clarendon, Oxford, England, U.K., 1904, p. 440.

[2] Bonnecaze, R. T., and Brady, J. F., "The Effective Conductivity of Random Suspensions of Spherical Particles," *Proceedings of the Royal Society of London, Series A*, Vol. 432, 1991, pp. 445–465.

[3] Choi, U. S., "Enhancing Thermal Conductivity of Fluids with Nanoparticles," *Developments and Applications of Non-Newtonian Flows*, Vol. 231, Fluid Engineering Division American Society of Mechanical Engineers, New York, 1995, pp. 99–105.

[4] Lee, S., and Choi, S. U. S., "Application of Metallic Nanoparticle Suspensions in Advanced Cooling Systems," *Recent Advances in Solids/Structures and Application of Metallic Materials*, PVP-Vol. 342/MD-Vol. 72, American Society of Mechanical Engineers, New York, Nov. 1996, pp. 227–234.

[5] Berber, S., Kwon, Y., and Tomanek, D., "Unusually High Thermal Conductivity of Carbon Nanotubes," *Physical Review Letters*, Vol. 84, No. 20, 2000, pp. 4613–4616.

[6] Fonseca, A., Hernadi, K., Piedigrosso, P., Colomer, J., Mukhopadhyay, K., Doome, R., Lazarescu, S., Biro, L., Lambin, P., Thiry, P., Bernaerts, D., and Nagy, J., "Synthesis of Single- and Multi-Wall Carbon Nanotubes over Supported Catalyst," *Applied Physics A*, Vol. 67, 1998, pp. 11–22.

[7] Dresselhaus, M. S., Dresselhaus, G., and Phaedon, A., *Carbon Nanotubes: Synthesis, Structure, Properties, and Applications*, Springer–Verlag, New York, 2001, pp. 29–31.

[8] Journet, C., and Bernie, P., "Production of Carbon Nanotubes," *Applied Physics A*, Vol. 67, 1998, pp. 1–9.

[9] Choi, S. U. S., Zhang, Z. G., Yu, W., Lockwood, F. E., and Grulke, E. A., "Anomalous Thermal conductivity Enhancement in Nanotube Suspensions," *Applied Physics Letters*, Vol. 79, No. 14, 2001, pp. 2252–2254.

[10] Xie, H., Lee, H., Youn, W., and Choi, M., "Nanofluids Containing Multiwalled Carbon Nanotubes and Their Enhanced Thermal Conductivities," *Journal of Applied Physics*, Vol. 94, No. 8, 2003, pp. 4967–4971.

[11] Wang, X., Xu, X., and Choi, U. S., "Thermal Conductivity of Nanoparticle-Fluid Mixture," *Journal of Thermophysics and Heat Transfer*, Vol. 13, No. 4, 1999, pp. 474–480.

[12] Lee, S., Choi, S. U. S., Li, S., and Eastman, J. A., "Measuring Thermal Conductivity of Fluids Containing Oxide Nanoparticles," *Transactions of the ASME: Journal of Heat Transfer*, Vol. 121, 1999, pp. 280–289.

[13] Xie, H., Wang, J., Xi, T., Liu, Y., and Ai, F., "Thermal Conductivity Enhancement of Suspensions Containing Nanosized Alumina Particles," *Journal of Applied Physics*, Vol. 91, No. 7, 2002, pp. 4568–4572.

[14] Assael, M. J., Chen, C. F., Metaxa, I., and Wakeham, W. A., "Thermal Conductivity of Suspensions of Carbon Nanotubes in Water," *International Journal of Thermophysics*, Vol. 25, No. 4, 2004, pp. 971–984.

[15] Wen, D. S., and Ding, Y. L., "Effective Thermal Conductivity of Aqueous Suspensions of Carbon Nanotubes (Carbon Nanotube Nanofluids)," *Journal of Thermophysics and Heat Transfer*, Vol. 18, No. 4, 2004, pp. 481–485.

[16] Jeffrey, D. J., "Conduction Through a Random Suspension of Sphere," *Proceedings of the Royal Society of London, Series A*, Vol. 335, 1973, pp. 355–367.

[17] Davis, R. H., "The Effective Thermal Conductivity of a Composite Material with Spherical Inclusions," *International Journal of Thermophysics*, Vol. 7, No. 3, 1986, pp. 609–621.

[18] Hamilton, R. L., and Crosser, O. K., "Thermal Conductivity of Heterogeneous Two-Component Systems," *Industrial and Engineering Chemistry Fundamentals*, Vol. 1, No. 3, 1962, pp. 187–191.

[19] Das, S. K., Putra, N., Thiesen, P., and Roetzel, W., "Temperature Dependence of Thermal Conductivity Enhancement for Nanofluids,"

Journal of Heat Transfer, Vol. 125, 2003, pp. 567–574.
[20] Challoner, A. R., and Powell, R. W., "Thermal Conductivities of Liquids: New Determinations for Seven Liquids and Appraisal of Existing Values," *Proceedings of the Royal Society of London, Series A*, Vol. 238, No. 1212, 1956, pp. 90–106.
[21] Vaccarini, L., Goze, C., Aznar, R., Micholet, V., Journet, C., and Bernier, P., "Purification Procedure of Carbon Nanotubes," *Synthetic Metals*, Vol. 103, 1999, pp. 2492–2493.
[22] Kukovecz, A., Kramberger, C., Holzinger, M., Kuzmany, H., Schalko, J., Mannsberger, M., and Hirsch, A., "On the Stacking Behavior of Functionalized Single-Wall Carbon Nanotubes," *Journal of Physical Chemistry B*, Vol. 106, No. 25, 2002, pp. 6374–6380.
[23] Dennison, J. R., Holtz, M., and Swain, G., "Raman Spectroscopy of Carbon Materials," *Spectroscopy (Amsterdam)*, Vol. 11, No. 8, 1996, pp. 38–46.
[24] Thomsen, C., "Raman Scattering in Carbon Nanotubes," *Proceedings of the International Society for Optical Engineering*, Vol. 5219, Nanotubes and Nanowires, edited by A. Lakhtakia and S. Maksimenko, International Society for Optical Engineering, Bellingham, WA, 2003, pp. 45–50.
[25] Tohji, K., Takahashi, H., Shinoda, Y., and Shimizu, N., "Purifying Single-Walled Nanotubes," *Nature (London)*, Vol. 383, No. 24, 1996, p. 679.
[26] Zhang, J., Zou, H., Qing, Q., Yang, Y., Li, Q., Liu, Z., Guo, X., and Du, Z., "Effect of Chemical Oxidation on the Structure of Single-Walled Carbon Nanotubes," *Journal of Physical Chemistry B*, Vol. 107, No. 16, 2003, pp. 37121–3718.
[27] Rinzler, A. G., Liu, J., Dai, H., and Nikolaev, P., "Large-Scale Purification of Single-Wall Carbon Nanotubes: Process, Product, and Characterization," *Applied Physics A*, Vol. 67, 1998, pp. 29–37.
[28] Chiang, I., Brinson, B. E., Smalley, R. E., Margrave, J. L., and Hauge, R. H., "Purification and Characterization of Single-Walled Carbon Nanotubes," *Journal of Physical Chemistry B*, Vol. 105, No. 6, 2001, pp. 1157–1161.
[29] Zhang, M., Yudasaka, M., Koshio, A., and Lijima, S., "Thermogravimetric Analysis of Single-Wall Carbon Nanotubes Ultrasonicated in Monochlolobenzene," *Chemical Physics Letters*, Vol. 364, 2002, pp. 420–426.
[30] Paredes, J. I., and Burghard, M., "Dispersion of Individual Single-Walled Carbon Nanotubes of High Length," *Langmuir*, Vol. 20, No. 12, 2004, pp. 5149–5152.
[31] Meyyappan, M., *Carbon Nanotubes Science and Applications*, CRC Press, New York, 2005.
[32] Incropera, F. P., and Dewitt, D. P., "Fundamentals of Heat and Mass Transfer," Wiley, New York, 2002.
[33] Howard, E., Unterweiser, P., Foster, J., Hontas, J., and Lyman, H., *Metal Handbook: Property and Selections*, 8th ed., American Society for Metals Intl., New York, 1973.
[34] Touloukin, Y. S., and Ho, C. Y., *Thermal Property of Matter*, The TPRC Data Series, Plenum, New York, 1970.
[35] Keblinski, P., Phillpot, S. R., Choi, S. U. S., and Eastman, J. A., "Mechanism of Heat Flow in Suspensions of Nano-Sized Particles (Nanofluids)," *International Journal of Heat and Mass Transfer*, Vol. 45, 2002, pp. 855–863.